Materials Science and Engineering B 322 (2025) 118663

Contents lists available at ScienceDirect

Materials Science & Engineering B

journal homepage: www.elsevier.com/locate/mseb

Al-fumarate/PVDF-HFP Mixed matrix membrane for water vapor adsorption in industrial drying processes

Marzia Pentimalli [a,*], Stefano De Antonellis [b], Maria Francesca Giuffrida [c], Andrea Martinelli [c], Luciano Pilloni [a], Franco Padella [d]

[a] ENEA Italian National Agency for Energy, New Technologies and Sustainable Economic Development, Department for Sustainability, Casaccia Research Centre, via Anguillarese 301, 00123 Rome, Italy
[b] Milan Polytechnic, Department of Energy, Campus Bovisa - Via Lambruschini, 4a - 20156 Milan, Italy
[c] Sapienza University of Rome, Department of Chemistry, Piazzale Aldo Moro 5, Rome 00185, Italy
[d] Independent author, member of the Italian Chemical Society (Società Chimica Italiana, SCI), Italy

ARTICLE INFO

Keywords:
Mixed Matrix Membrane
MOF
Water vapour adsorption
Drying processes

ABSTRACT

Metal Organic Frameworks (MOFs) are crystalline porous materials with high surface areas and tunable properties, making them ideal for dehumidification, water recovery, and thermal cooling applications. However, their powder form can limit practical use. Embedding MOFs in polymer matrices can be an effective way to obtain stable composite membranes while preserving adsorption performance.

This work focuses on the development of Aluminum-fumarate/poly(vinylidene fluoride-co-hexafluoropropylene) Mixed Matrix Membranes (MMM) for industrial drying cycles. Different membranes with 50–70 wt% MOF loadings were fabricated via solution casting. The effectiveness of the membranes was evaluated by measuring their specific surface area against that of pure MOF. The membrane containing 50 wt% Al-fumarate exhibited a low specific area of 390 m^2/g (normalized to the MOF content). Unexpectedly the membrane with the highest MOF content showed a drastic reduction in the specific area (170 m^2/g). The best performing sample resulted the 67 wt% MOF membrane, which achieved a specific area of 890 m^2/g. In this case, the embedded MOF particles retained about 90 % of the surface area of pure MOF (1010 m^2/g). Further in-depth analyses were conducted on this optimal sample allowing to assess its physical, mechanical, and functional properties. In particular, the water vapor adsorption capacity was found to be ~ 37 g_{H_2O}/g_{MOF} at p/p_0 0.9.

Using the simple methodology proposed, it was possible to develop a mixed matrix membrane that expresses the adsorption properties of the active material while solving powder management issues.

1. Introduction

Among the various classes of materials, Metal Organic Frameworks (MOFs) have gathered a significant attention due to their unique porous structure. These materials possess an ultrahigh surface area, which stems from their regular crystalline structure. This structural characteristic leads to a significant adsorption capacity. To optimize this property, the material performance can be tailored through several approaches: modifying its chemical and crystallographic structure, applying appropriate functionalization, or even designing new materials via synthesis from scratch. [1,2]. These characteristics give the materials the potential to be advantageously exploited in various technological applications. For example, but not only, MOFs have been positively applied in water purification or in carbon dioxide separation [3–5], in batteries for energy storage [6–8], in food packaging [9] and also in biomedical applications [10] when properly selected biocompatible building blocks are utilized in their synthesis.

MOFs containing light metals, such as aluminium, possess a remarkable water adsorption characteristic, that make them useful for a wide number of applications [11], in particular for water recovery and storage, dehumidification and for air conditioning and heat processing systems [12].

The agribusiness sector plays a relevant role in overall economic activities. With more than $13x10^6$ tons produced in the whole world in 2021 (about one third of this quantity was produced only in Italy) [13], the production of pasta represents one of the most relevant sectors in the

* Corresponding author.
E-mail address: marzia.pentimalli@enea.it (M. Pentimalli).

https://doi.org/10.1016/j.mseb.2025.118663
Received 13 February 2025; Received in revised form 29 July 2025; Accepted 1 August 2025
Available online 6 August 2025

agri-food industry. The pasta industry is an energy-intensive production, and the implementation of energy-efficient technologies can significantly affect the economic and environmental sustainability of the entire industry. The pasta drying stage requires high energy input, necessary to satisfy the high evaporation enthalpy of water. It has been evaluated that the energy required to desiccate the pasta during the drying process in air is about 60 % of the whole energy needed in the overall production process [14]. Therefore, recovery of heat from the humid air flow coming from the pasta drying stage can effectively generate a significant reduction in energy consumption, leading to a substantial increment in the process efficiency.

In previous work, aluminum fumarate (Al-fum) showed an effective performance in the recovery of low-grade waste heat ($\leq$100 °C) from industrial pasta drying processes [15,16]. Experimental tests in a pilot plant on a laboratory scale confirmed that the adsorption of water vapor from the dryer's humid exhaust air using a bed of Al-fum powder enables effective heat recovery through air recirculation (see Supplementary Information, the pasta drying process section). Despite material's effectiveness, however, practical challenges emerged in managing low-density MOF powder, particularly in fluidized-bed configurations. Powder dispersion and containment issues hampers scalability, making alternative approaches necessary. A viable solution is to move to a fixed-bed system by immobilizing Al-fum in a chemically and mechanically stable medium, preserving its adsorption properties.

The work addresses these challenges by developing an Al-fum/PVDF-HFP Mixed Matrix Membrane (MMM), a composite material in which MOF particles are uniformly dispersed in a polymer matrix at an optimized ratio. In the MMM, particle immobilization and adsorption retention must be balanced, ensuring mechanical stability, preventing powder from escaping and minimizing obstruction of the MOF's microporosity [17]. This can be obtained through careful control of MOF-polymer interactions and MOF to polymer ratio. Too weak interactions, in fact, can cause excessive particle agglomeration; conversely, strong interactions lead to pore clogging due to polymer overcoating. As for the polymer, excessive content can encapsulate particles and reduce their accessibility, while insufficient polymer leads to poor membrane handling.

The copolymer poly(vinylidene fluoride-co-hexafluoropropylene (PVDF-HFP) was selected as matrix material for the membranes due to its properties. Specifically, PVDF-HFP is hydrophobic, offering excellent chemical stability. These properties ensure compatibility with hydrophilic MOFs, such as aluminium fumarate [18]. As a result, degradation and adverse reactions during fabrication and operation can be minimized. Its fluorinated backbone can ensure adequate interfacial adhesion with Al-fum and resist pore clogging. The copolymer readily dissolves in various solvents. This solubility is critical, as it enables the material to be processed by solution casting. In the solid state, the copolymer exhibits flexibility due to the hexafluoropropylene blocks, which reduce crystallinity [19]. As a result, membranes derived from it are expected to be both mechanically robust and flexible. These properties allow them to withstand thermal cycling and mechanical stress.

A series of Al-fum/PVDF-HFP MMMs with MOF loadings between 50 and 70 wt% were prepared by a simple solution casting method. All membranes were preliminarily characterized to assess their suitability for water vapor adsorption. Surface area analyses by N_2 adsorption were compared with pristine Al-fum to evaluate porosity retention; morphological examination showed MOF particles and membrane microstructure. The analyses revealed the 67 wt% Al-fum/PVDF-HFP formulation as the best composition, due to the excellent surface area retention (~90 % of pristine Al-fum), indicating the accessibility of MOF porosities. This membrane was subjected to a comprehensive characterisation, including thermal analyses to assess thermal stability and phase transitions; mechanical tests to assess the possibility of handling under operating conditions; and surface wettability measurements to probe the hydrophilicity/hydrophobicity balance. Finally, water vapour adsorption isotherms at different temperature values provided preliminary performance data.

2. Experimental

2.1. Starting materials

Al-fum MOF, produced by MOFTechnologies ltd. (CAS 132041–53-3; MW = 158.05 g/mol; d = 0.71 g/ml), was purchased in powder form and used as received. As binding matrix, a polyvinylidene fluoride copolymer, namely poly(vinylidene fluoride-co-hexafluoropropylene) (PVDF-HFP), a statistically almost amorphous copolymer, was acquired in pellet form from Sigma-Aldrich (CAS 9011–17-0; number average molecular weight M_n = 130000; weight average molecular weight M_w = 400000; d = 1.77 g/cm^3). Dimethylformamide (DMF hereafter) (100 % from VWR Chemicals BDH®) was used as a solvent to prepare the polymeric solution.

2.2. Mixed matrix membranes preparation

The polymer/Al-fum Mixed Matrix Membranes were prepared through the sequential solution casting process reported in Fig. 1. Composition details are reported in Table 1. The initial step involved preparing a 10 % w/w PVDF-HFP solution by dissolving polymer pellets in DMF at 70 °C under continuous stirring for approximately 3 h, yielding a clear, homogeneous solution. Subsequently, predetermined quantities of Al-fum were incorporated into 10 cm^3 aliquots of the polymer solution and thoroughly homogenized using mechanical mixing in an agate mortar until achieving visually uniform white slurries. The slurries were observed under an optical microscope. Samples were found to be composed of uniformly distributed glomerates in the polymer solution. Quantitative microscopy showed a log-normal distribution with a mean diameter of approximately 7 μm (see Supplementary information). Resulting mixtures were then cast onto glass substrates within 3 cm × 10 cm mylar frames, using a blade to adjust the thickness. To ensure controlled solvent evaporation, the cast slurries were left to dry overnight at room temperature (~20 °C). This gradual drying process produced freestanding membranes with thicknesses ranging between 200–400 μm. Following solvent evaporation, the dried membranes were carefully peeled from the glass substrates and weighted for further characterization. Two replicate films were prepared for each composition to ensure reproducibility (see Supplementary information for the step-by-step protocol).

2.3. Mixed matrix membranes characterization

Prepared samples were analyzed to assess the adsorption behavior of the MOF dispersed phase. A more in-depth analysis was carried out on the best performing sample. In details:

– N_2 adsorption isotherms at 77 K were collected by Autosorb iQ30 instrument by Quantachrome, after 8 h outgassing at 100 °C under vacuum. Specific Surface Area (SA) of samples were calculated by applying the Brunauer, Emmet, Teller (BET) equation [20]; cumulative pore volume and pore size distributions were calculated by applying the Horvath-Kawazoe (HK) model [21].

– Morphological characterizations were performed by Field Emission scanning electron microscope (FE-SEM) analysis using a ZEISS LEO 1530 and a ZEISS AURIGA SEM apparatus at very low voltage. Samples were fixed on the stubs using a graphite-based conductive adhesive.

– Mechanical properties were obtained by tensile stress–strain experiments. Tests were carried out using an Instron 4502 instrument equipped with a 10 N cell. The dumbbell dog bone specimens were die-cut from casted films, according to ASTM D638 standard, and elongated at 5 mm min^{-1}. Stress–strain curves were reported as the apparent stress F/A, where F is the tensile force and A is the initial cross-sectional area of each test specimen, versus the strain $(L-L_0)/L_0$, where L_0 and L are the initial and the deformed sample length, respectively. The Young

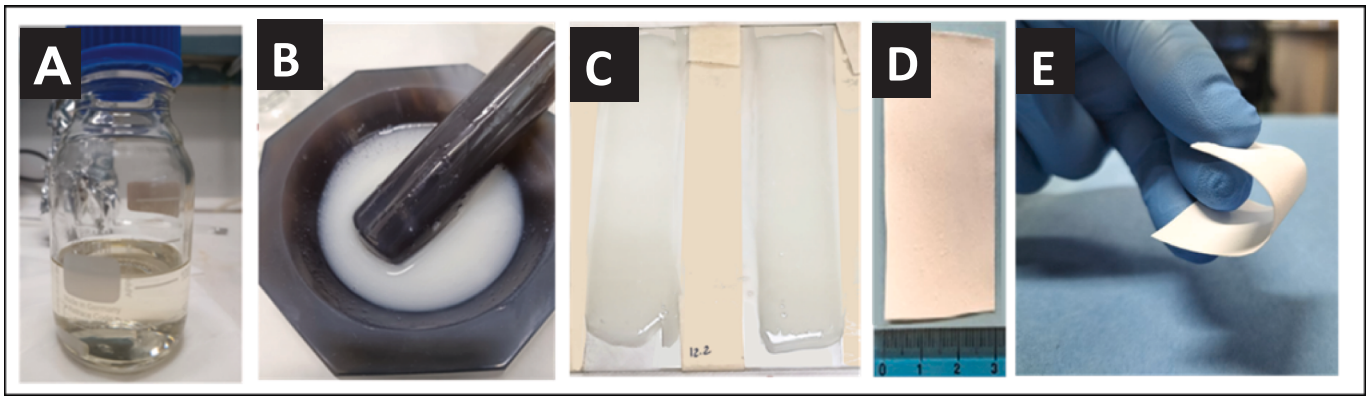

Fig. 1. Procedural sequence followed to obtain Al-fum/PVPDF-HFP Mixed Matrix Membrane. From A to E: PVPDF-HFP polymer solubilization into DMF (10% wt. ratio); Al-fum mechanical dispersion and homogenization into PVPDF-HFP DMF solution; casting on a glass plate; MMM after desiccating stage.

Table 1
Experimental details of composite membranes compositions.

Sample id	*MOF content*		*MOF to polymer*	*MOF to polymer*
	wt%	*vol%*	*weight ratio*	*volume ratio*
M50	50	72	1.00:1	2.57:1
M60	60	79	1.50:1	3.76:1
M65	65	82	1.86:1	4.56:1
M67	67	83	2.03:1	4.88:1
M70	70	85	2.31:1	5.67:1

modulus (E_y) was calculated from the slope of the initial linear region of the stress–strain curves while the tensile strength (TS) was taken at the maximum stress, occurring at the break point at a strain ε_b. The reported results are the mean values ± maximum error on three-times experiments.

– Thermal analyses were carried on by Differential scanning calorimetry (DSC). Measurements were performed by using a Mettler Toledo DSC 822e instrument. The analyses were carried out in nitrogen flow at 20 ml/min on about 6–9 mg of sample. The applied temperature program consisted in a) a heating scan at 10 °C/min from 0 to 200 °C (1st heating); b) a cooling at 30 °C/min from 190 to 25 °C; c) a heating scan from 25 to 200 °C at 10 °C/min (2nd heating).

– Water wettability was evaluated by static contact angle (SCA) measurements, performed by depositing 5 μL of Milli-Q water onto vacuum-dried samples. SCAs were calculated using Motic Image Plus 2.0 software. The reported contact angles represent the average of measurements taken from at least 5 different drops. A series of images was acquired sequentially over a 20-minute period following the drop deposition for the evaluation of SCA and drop volume variation. The volume was determined considering the drop as a spherical cap.

– Water vapour adsorption analyses were conducted by using the Aquadyne DVS2 Dynamic Vapour Sorption thermogravimetric balance. The MMM film and pure Al-fum powder were simultaneously analysed and compared. An initial treatment in nitrogen flow at 85 °C for 10 h is carried out to remove residual moisture in the sample. Then, the chamber is cooled to the temperature of the experiment and then the relative humidity is started to increase in 10 % increments. Water vapour adsorption measurements were made at 65 °C and 45 °C at increasing relative humidity and the change in mass of the materials was measured.

All the above characterizations were performed on at least two replicate samples to verify reproducibility. The reported data represent average values unless otherwise specified.

3. Results and discussion

3.1. Preliminary analyses

All the obtained membranes appear macroscopically homogeneous as shown in Fig. 1D. A diffuse micrometric porosity, produced during the drying stage, can be observed on the surface (see Fig. 2). XRD analysis revealed the effectiveness of the preparation process to obtain MMM composites without any significant phase change in the Al-fum, being the polymer traces fully dispersed in the background. In all samples, in fact, reflections of the MOF phase strongly overlap the prevalently amorphous signals of the binding polymer (see supplementary information).

FTIR analysis shows that absorption spectra of the developed composite membranes derive from the simple sum of PVDF-HFP and MOF pristine characteristics, indicating the absence of significative chemical interactions between membrane components (see details in supplementary information).

Samples containing 50–67 wt% Al-fum loading present good handling characteristics (see Fig. 1E). The M70 film shows a more brittle behavior, not allowing an easy manipulation without breaking down.

In Fig. 3 representative SEM images of MOF particles and composite films are shown. While M50 and M67 images (Fig. 3B and 3C respectively), are clearly due to the irregular surface of the polymeric material that surrounds MOF particles, the M70 image (Fig. 3D) evidences the polyhedral forms of the crystalline Al-fum particles and glomerates scarcely bound by the PVPDF-HFP polymer.

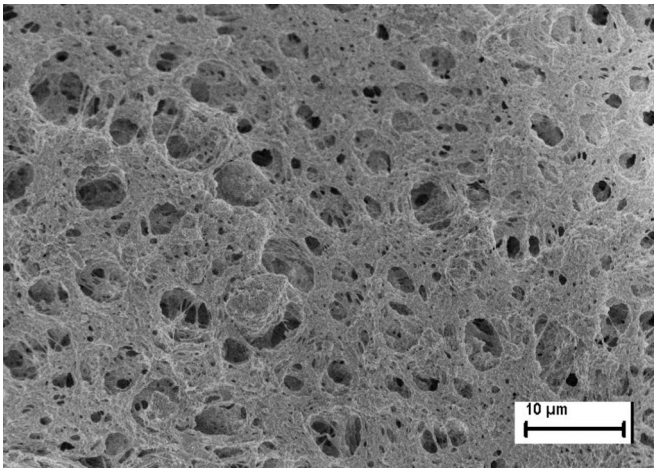

Fig. 2. Representative image of the membrane surface (SEM image in in-lens mode).

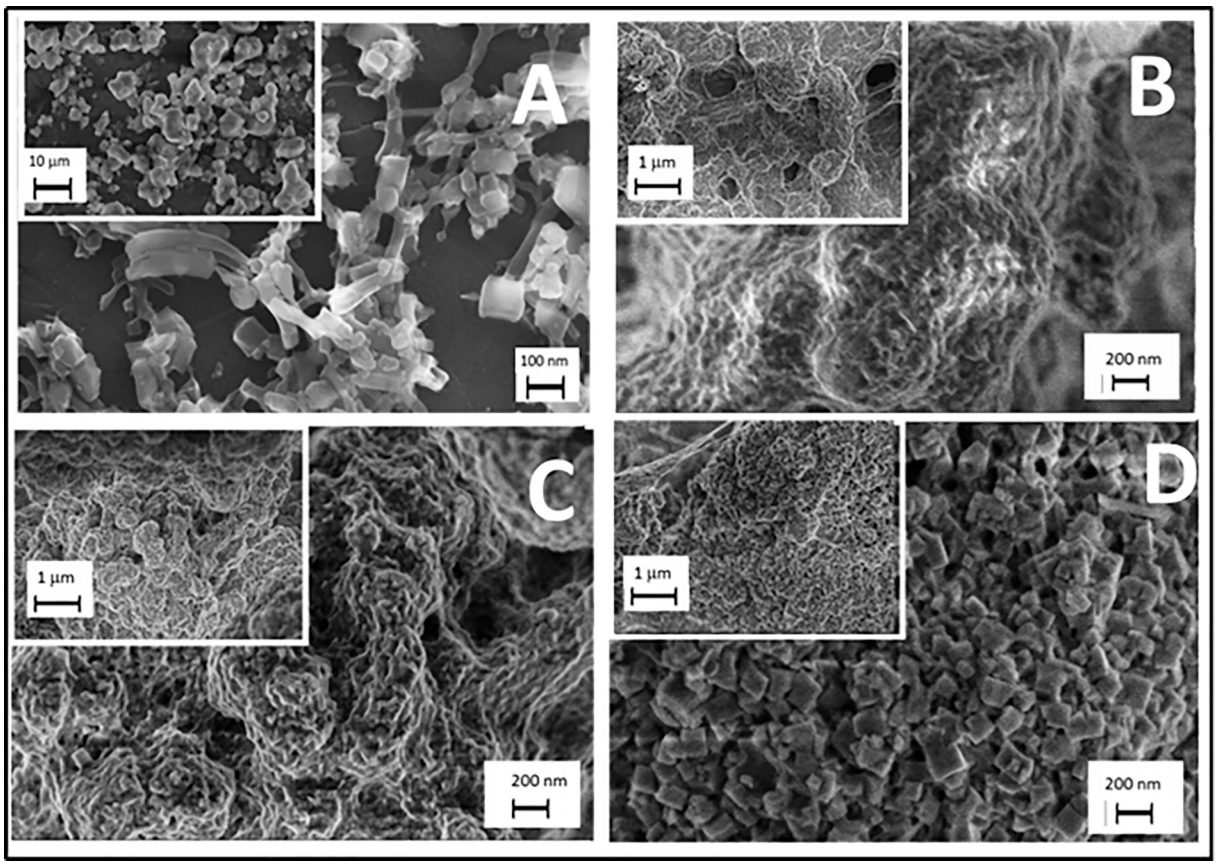

Fig. 3. SEM images of pure Al fumarate and representative samples of Al-fum/PVPDF-HFP Mixed Matrix Membranes. A) Al-fum particles; B) M50; C) M67; D) M70.

The screening analysis continued by evaluating the specific surface area of the composite membranes as a function of their MOF content. All the samples were subjected to nitrogen adsorption measurements at 77 K including the pristine Al-fum MOF in powder form as reference. The BET analysis results, reported in Table 2, evidence that all samples show a decreasing in normalized surface area, as a consequence of a variable degree of pore occlusion that occurs. However, the decrease of the specific area values does not appear to follow a simple linear relationship with MOF content in the composite materials. The pure material exhibits a specific surface area of 1010 m^2/g. The MOF in M60, M65 and M67 samples, possesses normalised specific areas of 820, 800 and 890 $m^2/g_{Al\text{-}fum}$. The BET analysis of the M50 membrane furnishes a low specific area (390 $m^2/g_{Al\text{-}fum}$), related to the occlusion effect on MOF pores promoted by the relatively large content of polymer (28 % by vol.), enough to produce a non-negligible particles incorporation. Surprisingly, the M70 film, containing the lowest polymer amount, shows an unexpected dramatic falling in its normalized area, as low as 170 $m^2/g_{Al\text{-}fum}$. The anomalous value requires a confirm by excluding the hypotheses of a structural collapse or loss in mass content of the active material.

Table 2
Specific Surface Area from BET Analysis.

Sample	*Surface Area* (m^2/g_{film})	*Normalized Surface Area* ($m^2/g_{Al\text{-}fum}$)
Al-fum	1010 ± 30	1010 ± 30
M50	195 ± 7	390 ± 20
M60	493 ± 10	820 ± 20
M65	520 ± 10	800 ± 10
M67	590 ± 10	890 ± 20
M70	120 ± 20	170 ± 20

4. The M70 Mixed matrix membrane

Structural and microstructural characteristics of the prepared composite samples were inferred by XRD data. Any significant changes in structural parameters occurred. From a microstructural point of view, a slight improvement in the average grain size is observed in M70 sample (314Å vs 285Å of the pure MOF). In addition, the dispersed MOF phase exhibits a lower microstrain value (0.3 % vs 0.7 %). The correspondence of the nominal chemical composition was also confirmed by measuring the Al_2O_3 residue in a high temperature thermogravimetric analysis (see Supplementary Information).

From analytical results, it can certainly be ruled out that the unexpectedly low value of the surface area can be related neither to a collapse of the MOF structure nor to any loss from the membrane.

SEM analysis reported in Fig. 3, provide further elements for discussion. The M50 sample (Fig. 3B) shows that PVPDF-HFP polymer significantly incorporates crystalline MOF particles, despite its minor volumetric ratio (that is about 1/3 of MOF volume). The M67 sample (Fig. 3C), that possess the best value in surface area, exhibits a surface morphology composed of multiple almost parallel layers of polymeric thin films. The polyhedral geometries of the MOF glomerated particles remain clearly visible in the M70 sample (Fig. 3D).

4.1. Our hypothesis: Competing forces

In the MMM development stage, the Al-fum component is dispersed in a slurry in which the DMF polymer solution completely wets the MOF particles. In the subsequent drying step, slow evaporation of the solvent occurs. As a result, the solute concentration increases and the polymer begins to solidify, forming solvent-saturated percolating structures around the MOF particles. Subsequently, further evaporation of the solvent promotes consolidation of the precipitate, which seeks to

stabilize a solidified, solvent-free network structure that incorporates MOF particles. At this point, mechanical micro-stresses appear, due to competitive forces resulting from polymer shrinkage (due to solvent loss) and interfacial adhesive forces acting on polymer molecules that adheres to glomerated particle surfaces [22]. As a consequence of the randomly oriented dispersion of MOF particulate, tension acts in the whole body of the MMM in formation. Three different situations can occur at this stage:

i) when the polymer content is sufficient, the contraction forces can overcome the interfacial forces. In this case, the polymer shrinks freely. However, the surfaces of the dispersed particles remain occluded, due to the additional input of other solvent-saturated polymeric material from the surrounding environment. The consolidation process proceeds and the MOF particles remain fully embedded in the polymer. As a result, significant occlusion of the porosity occurs and the measured normalized specific area of MOF drops. This is the case for sample M50 (see the image in Fig. 3B and the specific area values in Table 2).

ii) At lower polymer content, mechanical micro-stresses can be produced by nearly equivalent contraction and interfacial forces. In this case, evaporation of the solvent that permeates the precipitated polymer can promote both separation of the polymer from the particle surface and disruption of areas of the forming polymer network. Coupled phenomena can create pathways to particles surfaces as well as release of particles surfaces porosity. An increased specific area of the MOF material is measured. This is the case with samples M60, M65 and M67 (see Fig. 3C and Table 2).

iii) When the polymer content is minimal, the interfacial adhesive forces can overcome the shrinking forces. The layer of precipitated polymer remains adhered in a film form on the glomerated particles surface.

The three-dimensional polymeric network around the MOF particulate is brittle, coming from the sole contact points allowed by the geometry of the underlying MOF particles (see Fig. 3D). Counter-intuitively, there is again a significant decrease in the measured specific area. This is the case with sample M70: the polymer occludes the surface porosity of the Al-fum particles and the measured surface area decreases (see Table 2).

From the above analysis, the best performing sample was found to be the M67 membrane, which exhibits a minimal degree of pore occlusion and easy handling without breakage (see Fig. 1E). Therefore, the M67 mixed-matrix membrane was subjected to further characterization and the results are shown below.

5. The M67 Mixed matrix membrane

a) N_2 Adsorption isotherms.

In Fig. 4 the full N_2 adsorption isotherm of the composite, measured at 77 K, is compared to that one of pristine aluminium fumarate. Samples exhibit similar curves, corresponding to a type I + II isotherm, according to the IUPAC classification. In the case of the MMM, the transition from microporous to mesoporous adsorption (i.e. the point where the knee is formed) appears at ~ 110 cm^3/g of nitrogen adsorption @STP (i.e. 0 °C and 1 atm). The value is about the half of the corresponding value of the pure Al-fum material, as a result of the occlusion effect on MOF porosity due to the polymeric phase. In the entire mesoporous branch of the isotherm the observed increase in the nitrogen adsorption of the MMM is about the half of the analogous increase of the MOF curve. This is again related to the occluding effect of the polymer on particles pores. The Fig. 5 shows the cumulative volume and pore size distribution comparisons, obtained by applying the HK model to the isotherms. The pore size distribution of the composite is centred at 2.54 Å radius value, a value corresponding to that of the pure MOF. Consistently with the role of porosity hindrance played by the polymer on the surface of MOF particles, the observed value of the cumulative volume in the MMM sample is lower than that resulting from pure Al-fum powder (0.21 cm^3/g versus 0.42 cm^3/g for the composite and pure material, respectively).

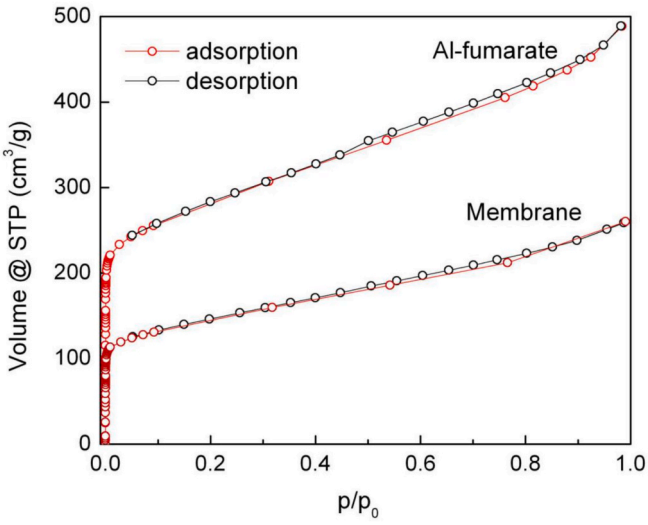

Fig. 4. Nitrogen adsorption isotherm at 77 K of Aluminium fumarate and M67 sample.

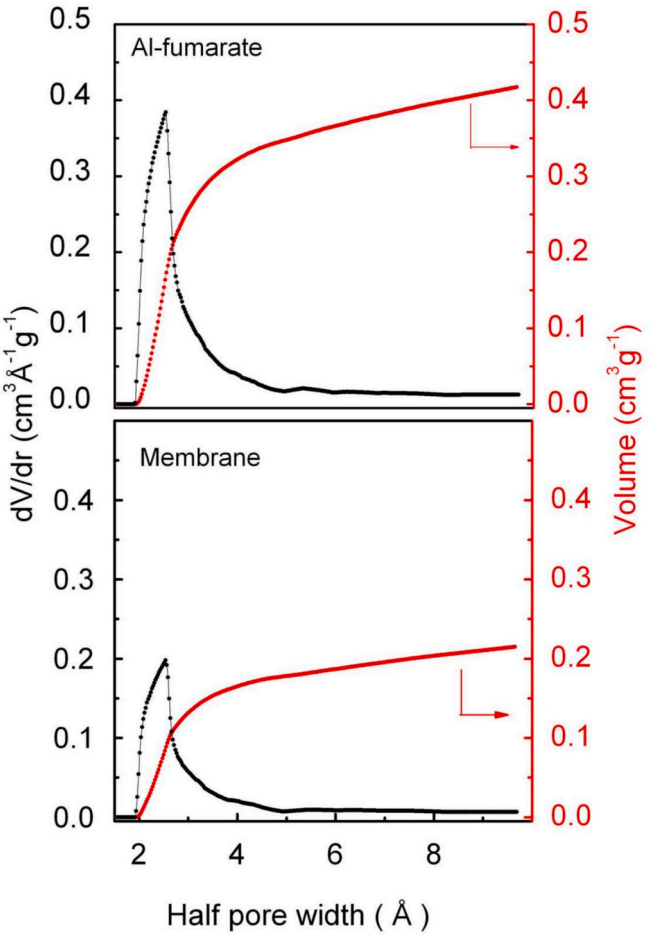

Fig. 5. Cumulative pore volume and pore size distribution of Al-fum powder (top) and M67 sample (bottom) obtained through the HK method. The pore size distribution is centred at 2.54 Å for both sample; Cumulative volume values are 0.42 and 0.21 cm^3/g for Al-fum and M67, respectively.

b) Thermal analysis.

Comparison in DSC analyses of a pure PVDF-HFP film and the composite M67 membrane were carried out to evidence possible differences in polymer behaviour deriving by the Al-fum MOF dispersion.

The DSC curves of the samples acquired in the first heating, cooling, and second heating cycles are reported in Fig. 6 A, B and C, respectively. In all the cases, the heat flow was normalized with respect to the PVDF-HFP weight content.

The thermal properties of PVDF-HFP and M67 samples evaluated from DSC experiments are reported in Table 3. PVDF-HFP film shows a melting peak centred at 146 °C characterized by enthalpy of fusion of 34.5 J g^{-1} from which a crystallinity of $X_c = 33$ wt%, slightly higher than that one found in pure polymer sample casted from dimethylacetamide solution ($X_c = 23.7$) [23].

As far as the M67 sample, the intense endothermic peak observed in the first heating, centred at 104 °C and spanning in a wide temperature range, is due to the evaporation of water absorbed from the environment, partially hiding the PVDF-HFP melting process (to facilitate comparison, the heat flow of the DSC curve of M67 in Fig. 6A was reduced by a factor of 5).

From peak integration between 0 °C and 130 °C and considering the enthalpy of water evaporation ($\Delta H_{vap} = 2260$ Jg^{-1}), it can be inferred that the M67 sample absorbed approximately 14 wt% of water from the environment. After the first heating cycle the samples were cooled at room temperature and reheated. Fig. 6B shows the exothermic peaks of the polymer melt crystallization. The nearly identical temperatures at which crystallization occurs (see Table 3) indicate that the MOF within the composite membrane did not exhibit any nucleating activity for the polymer matrix. The presence of MOF, however, inhibited crystallization. As a result, sample M67 exhibited both a lower ΔH_c and a broader exothermic peak at lower temperatures relative to the pure polymer. These differences were evident in the subsequent heating scan. The absence of water evaporation allowed for a direct analysis of the M67 melting process. Unlike PVDF-HFP, the composite membrane displayed a double melting process. This behaviour likely results from either PVDF-HFP's polymorphic structures or the melting-recrystallization of imperfect crystals at elevated temperatures. Analysis of the melting behaviour also revealed a slight decrease in PVDF-HFP crystallinity due to the addition of Al-fumarate, consistent with the findings of Cheng et al. in the case of PVDF/Al-fum at higher MOF concentration [24].

c) Mechanical Properties.

Mechanical properties of PVDF-HFP film and M67 membrane were analysed by tensile stress–strain experiments. The results are displayed in Fig. 7 for representative specimens. The mechanical features obtained from the stress–strain curves are reported in Table 4.

The addition of MOF to PVDF-HFP has a reinforcing effect at low elongations, as evidenced by the substantial increase in membrane Young modulus E_y. Conversely, at higher deformations, a reduction in tensile strength (TS) and elongation at break of the composite membrane compared to the pure polymer is observed.

Table 3
Thermal properties of PVDF-HFP and M67 samples.

sample	*1st heating*		*cooling*		*2nd heating*		
	T_m (°C)	ΔH_m (J g^{-1})	T_c (°C)	ΔHc (J g^{-1})	T_m (°C)	ΔH_m (J g^{-1})	X_c (wt %)
PVDF-HFP	145	34.5	110	38.28	110	40	38
M67	144	1260 [a]	109	23	127-141 [b]	29	28

[a] evaluated from 0 °C to 134 °C
[b] first and second melting peak

The mechanical properties of the composite derive from the interaction between two factors, the porous structure and the incorporation of Al-fum particles. The micro-porosities (Fig. 7B) within the composite matrix increase local mechanical stress due to stress concentration effects. This explains the behavioural difference between the mechanical characteristics of the polymeric matrix and the composite. In fact, the Al-fum particles (having a high elastic modulus [25]) reinforce the material by increasing stiffness in the first stages of deformation (elastic zone). Above a certain load due to the phenomenon of local stress concentration, the total strength decreases compared to that of the polymer alone.

d) Wettability.

The behaviour of the developed composite membrane with respect to its interaction with water was examined by evaluating surface wettability of the material. To evaluate surface wettability, Static Contact Angles (SCAs) were measured by processing the images of water droplets deposited on the pure PVDF-HFP matrix and M67 samples. As expected, the compact PVDF-HFP surface exhibited hydrophobic behaviour, as indicated by its high SCA of 114° ± 1°, consistent with literature data [26]. The sample exhibits a slightly higher value of SCA (120° ± 1°), probably due to an increased surface roughness. Time-dependent image acquisition on the composite revealed a minimal decrement of SCA combined with a consistent decrease of droplet volume as shown in Fig. 8.

Wettability critically governs the interaction between water and the membrane surface, especially when the material temperature drops below the dew point. A low contact angle (i.e. less than 90°), corresponds to the formation of a thin layer of liquid water on the membrane surface, affecting in this way vapor adsorption efficiency. In contrast, the high contact angles observed in the MMM leads to discrete droplets that minimize surface coverage, preserving active sites for vapor-phase

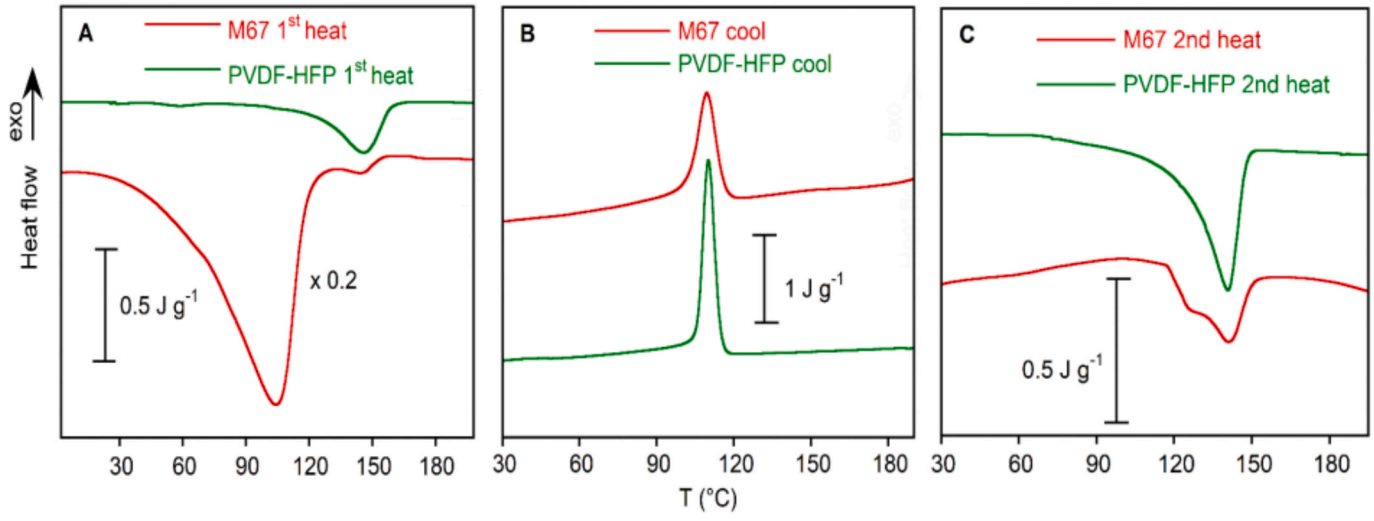

Fig. 6. DSC thermograms of PVDF-HFP and M67 samples. A) First heating; B) cooling, C) second heating. The heat flow is normalized with respect of the PVDF-HFP weight. For sake of comparison, the heat flow of the first heating of M67 is multiply for a 0.2 factor.

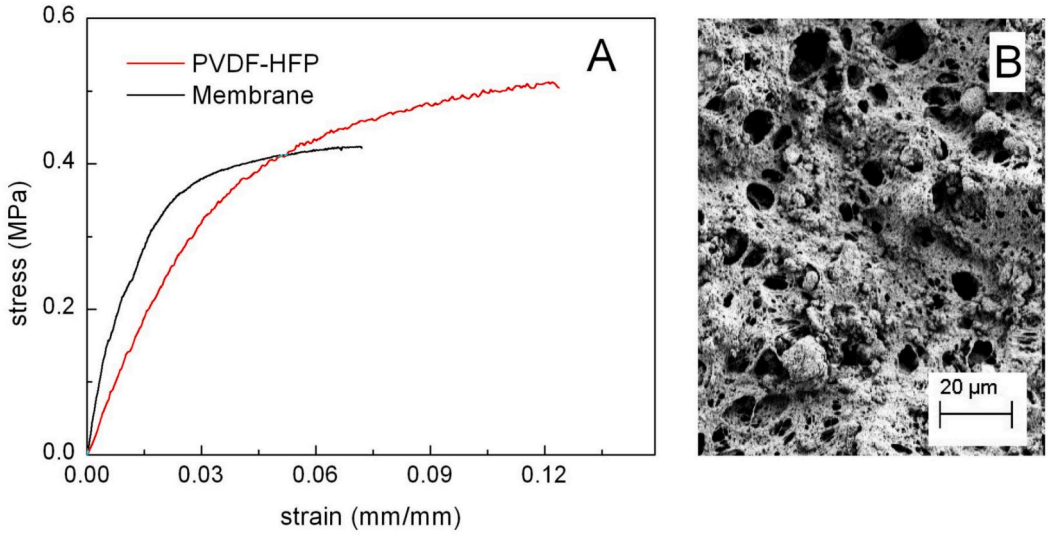

Fig. 7. A) Tensile stress–strain curves of PVDF-HFP and M67 films. B) SEM image of the fracture surface.

Table 4
Mechanical properties of PVDF-HFP and M67 membrane.

sample	E_y *(MPa)*	*TS (MPa)*	ε_b
PVDF-HFP	11.0 ± 0.4	0.50 ± 0.08	0.12 ± 0.02
M67	28.5 ± 0.2	0.42 ± 0.04	0.07 ± 0.02

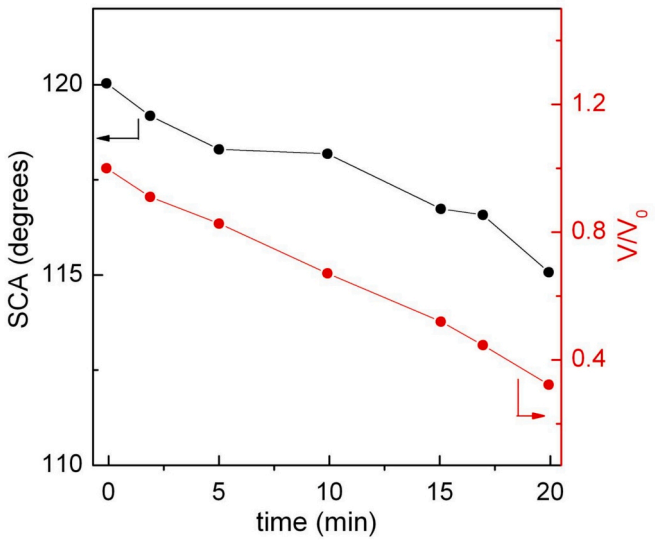

Fig. 8. Static contact angle (SCA) and water drop volume on M67 membrane as a function of time.

adsorption. The observed halving in droplet volume can be attributed to rapid evaporation facilitated by the hydrophobicity of PVDF-HFP.

In the proposed dehumidification processes, this behaviour enables the composite membrane to exploit its hydrophobic surface properties, thereby preventing liquid clogging while ensuring the dispersed MOF porosity remains fully effective for vapor capture.

e) Water vapor adsorption

The water adsorption isotherms of the M67 membrane at 65 °C and 45 °C were collected by using a gravimetric system and compared with the identical adsorption measurements performed on the pure Al-fumarate powder. The results are reported in Fig. 9. As expected, the composite shows a water adsorption capacity lower than the one resulting from the pure Al-fum. This trend is in accordance with the

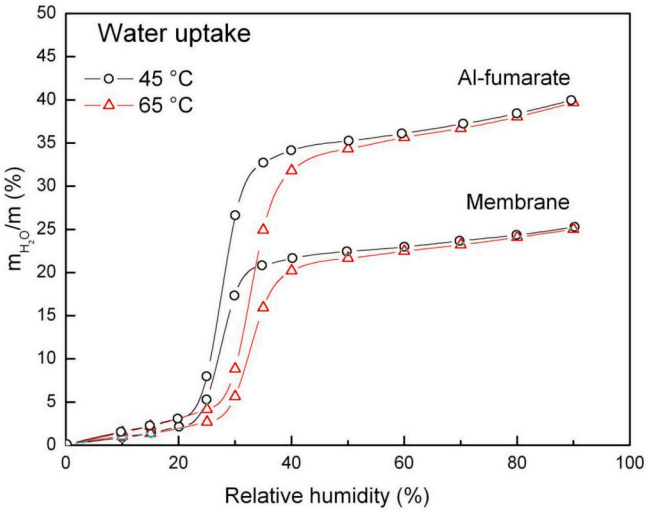

Fig. 9. Water adsorption isotherms at 65 °C and 45 °C of M67 mixed matrix composite, in comparison with the Al-fumarate powder.

experimental nitrogen adsorption data. By normalizing the adsorption data, it is possible to state that more than 90 % of the sorbent MOF properly works when included in the compound. The adsorption isotherms exhibit identical temperature dependence for pure Al-fumarate and the membrane, indicating that polymer-MOF interactions preserve the MOF's Type V isotherm (IUPAC) behavior. From observed behavior no variations are expected out from the tested range.

6. Conclusions

This work successfully developed an innovative Mixed Matrix Membrane composed of Aluminum fumarate embedded in a PVDF-HFP polymer matrix, designed for applications in dehumidification, water recovery, and thermal cooling. The membrane was fabricated via a simple and scalable solution casting process, effectively combining the high-water vapor adsorption capacity of the MOF with the mechanical stability, processability, and hydrophobicity of the polymer. Compared to pure polyvinylidene fluoride, the incorporation of hexafluoropropylene comonomer in the PVDF-HFP copolymer significantly reduces crystallinity, thereby advantageously enhancing the material's flexibility and processability.

The optimized membrane, containing 67 wt% Al-fum, demonstrated high performance by retaining 90 % of the MOF's original surface area (890 vs 1010 m2/g_{MOF}). This composition ensured effective embedding of MOF particles while avoiding pore occlusion, striking an ideal balance between adsorption capacity and structural integrity. The water adsorption isotherms exhibited the characteristic type V behavior of pure Al-fum, with only a minor reduction in the water uptake capacity (37.3 vs. 40 g_{H_2O}/g_{MOF} at $P/P_0 = 0.9$). Furthermore, the membrane maintained its temperature-dependent adsorption properties (45–65 °C), proving that the polymer-MOF interaction doesn't modify the sorption behavior of the compound.

The use of hydrophobic PVDF-HFP matrix in MMMs beneficially helps prevent liquid water accumulation below the dew point, while still permitting the embedded Al-fum particles to maintain their vapor adsorption capability. In addition, the micrometric porosity of the membranes obtained by casting allows free access for vapor to the active sites of the MOF.

Membranes with higher Al-fum loadings (e.g. 70 wt%) exhibit a drastic reduction in surface area (170 m^2/g) due to the occlusion of the MOF pores by the polymer component. The effect occurs when the polymer content is minimal and interfacial adhesive forces dominate over contraction forces, maintaining a thin, continuous film of precipitated polymer molecules adhered to the surfaces of MOF particles. This suggests the presence of a critical composition threshold and emphasizes also the importance of interfacial optimization in MMM design.

The proposed fabrication strategy can constitute an advancement in integrating powder MOFs into practical applications for dehumidification, water recovery, and thermal cooling. Future research will pursue complementary objectives such as study of water vapor adsorption kinetics and long-term cycling stability in the membrane systems and engineering a functional desiccant module system to validate its performance under realistic operating conditions.

CRediT authorship contribution statement

Marzia Pentimalli: Writing – review & editing, Writing – original draft, Supervision, Methodology, Investigation, Conceptualization. **Stefano De Antonellis:** Investigation. **Maria Francesca Giuffrida:** Investigation, Data curation. **Andrea Martinelli:** Investigation. **Luciano Pilloni:** Investigation, Conceptualization. **Franco Padella:** Writing – review & editing, Supervision, Data curation, Conceptualization.

Declaration of competing interest

The authors declare that they have no known competing financial interests or personal relationships that could have appeared to influence the work reported in this paper.

Appendix A. Supplementary data

Supplementary data to this article can be found online at https://doi.org/10.1016/j.mseb.2025.118663.

Data availability

Data will be made available on request.

References

[1] H.C. Zhou, J.R. Long, O.M. Yaghi, Introduction to Metal-Organic Frameworks, Chem. Rev. 112 (2) (2012) 673–674, https://doi.org/10.1021/cr300014x.

[2] M. Safaei, M.M. Foroughi, N. Ebraimpoor, S. Jahani, A. Omidi, M. Khatami, A review on metal-organic frameworks: Synthesis and applications, TrAC Trends in Anal. Chem. 118 (2019) 401–425, https://doi.org/10.1016/j.trac.2019.06.007.

[3] A. Haruna, Z.U. Zango, G. Tanimu, T. Izuage, S.G. Musa, Z.N. Garba, Z.M. A. Merican, A critical review on recent trends in metal-organic framework-based composites as sustainable catalysts for environmental applications, J. Env. Chem. Eng. 12 (5) (2024) 113542, https://doi.org/10.1016/j.jece.2024.113542.

[4] S.K. Firooz, D.W. Armstrong, Metal-organic frameworks in separations: a review, Anal. Chim. Acta 1234 (2022) 340208, https://doi.org/10.1016/j.aca.2022.340208.

[5] Y. Duan, L. Li, Z. Shen, J. Cheng, K. He, Engineering Metal-Organic-Framework (MOF)-based Membranes for Gas and Liquid Separation, Membranes 13 (5) (2023) 480–510, https://doi.org/10.3390/membranes13050480.

[6] J.C. Barbosa, R. Gonçalves, A. Valverde, P.M. Martins, V.I. Petrenko, M. Márton, A. Fidalgo-Marijuan, R.F. de Luis, C.M. Costa, S. Lanceros-Méndez, Metal organic framework modified poly(vinylidene fluoride-co-hexafluoropropylene) separator membranes to improve lithium-ion battery capacity fading, Chem. Eng. J. 443 (2022) 136329, https://doi.org/10.1016/j.cej.2022.136329.

[7] G. Tatrari, R. An, F.U. Shah, Designed metal-organic framework composites for metal-ion batteries and metal-ion capacitors, Coord. Chem. Rev. 512 (2024) 215876, https://doi.org/10.1016/j.ccr.2024.215876.

[8] X. Hou, J. Sun, M. Lian, Y. Peng, D. Jiang, M. Xu, B. Li, Q. Xu, Emerging Synthetic Methods and applications of MOF-Based Gels in Supercapacitors, Water Treatment, Catalysis, Adsorption, and Energy Storage, Macromol. Mater. Eng. 308 (2023) 2200469, https://doi.org/10.1002/mame.202200469.

[9] Y. Fu, D. Yang, Y. Chen, J. Shi, X. Zhang, Y. Hao, Z. Zhang, Y. Sun, J. Zhang, MOF-Based active packaging Materials for Extending Post-Harvest Shelf-Life of Fruits and vegetables, Materials 16 (9) (2023) 3406, https://doi.org/10.3390/ma16093406.

[10] S. Kundu, A.K. Swaroop, J. Selvaraj, Metal-Organic Framework in Pharmaceutical Drug delivery, Curr. Top. Med. Chem. 23 (13) (2023) 1155–1170, https://doi.org/10.2174/1568026623666230202122519.

[11] W. Fan, K.Y. Wang, C. Welton, L. Feng, X. Wang, X. Liu, Y. Li, Z. Kang, H.C. Zhou, R. Wang, D. Sun, Aluminum metal–organic frameworks: from structures to applications, Coord. Chem. Rev. 489 (2023) 215175, https://doi.org/10.1016/j.ccr.2023.215175.

[12] S. Gökpinar, S.J. Ernst, E. Hastürk, M. Möllers, I. El Aita, R. Wiedey, N. Tannert, S. Nießing, S. Abdpour, A. Schmitz, J. Quodbach, G. Füldner, S.K. Henninger, C. Janiak, Air-con Metal–Organic Frameworks in Binder Composites for Water Adsorption Heat Transformation Systems, Ind. Eng. Chem. Res. 58 (47) (2019) 21493–21503, https://doi.org/10.1021/acs.iecr.9b04394.

[13] T. Ozbun (2023, May 2), Global pasta production 2021, by country [Infographic]. Statista https://www.statista.com/statistics/1378224/leading-countries-worldwide-in-pasta-production/.

[14] L. Ozgener, O. Ozgener, Exergy analysis of industrial pasta drying process, Int. J. Energy Res. 30 (2006) 1323–1335, https://doi.org/10.1002/er.1227.

[15] S. Bellocchi, G.L. Guizzi, M. Manno, M. Pentimalli, M. Salvatori, A. Zaccagnini, Adsorbent materials for low-grade waste heat recovery: Application to industrial pasta drying processes, Energy 140 (2017) 729–745.

[16] G.L. Guizzi, M. Manno, A. Zaccagnini, M. Salvatori, S. Bellocchi. Sistema dimostrativo STEAM per il recupero energetico da cascami termici a bassa temperatura. Prove cicliche di lunga durata e con cicli parziali. Report RdS/PAR2018/078 (2018). https://www.ricercasistemaelettrico.enea.it/archivio-documenti.html?task=download.send&id=3990:sistema-dimostrativo-steam-per-il-recupero-energetico-da-cascami-termici-a-bassa-temperatura-prove-cicliche-di-lunga-durata-e-con-cicli-parziali&catid=146 (accessed on 27 December 2024).

[17] J. Dechnik, J. Gascon, C.J. Doonan, C. Janiak, C.J. Sumby, Mixed-Matrix Membranes, Angew. Chem. Int. Ed. 56 (2017) 9292–9310, https://doi.org/10.1002/anie.201701109.

[18] M. Pentimalli, A. Aliboni, M. Bellusci, A. La Barbera, F. Padella, L. Pilloni, F. Varsano. Sviluppo di un composito a matrice polimerica ad alto caricamento di MOF. Prove di fattibilità e valutazioni esplorative. Report RdS/PAR 2018/077 (2018). https://www2.enea.it/it/Ricerca_sviluppo/documenti/ricerca-di-sistema-elettrico/adp-mise-enea-2015-2017/processi-e-macchinari-industriali/report-2018/rds-par2018-077.pdf (accessed on 27 December 2024).

[19] P. Martins, A.C. Lopes, S. Lanceros-Mendez, Electroactive phases of poly (vinylidene fluoride): Determination, processing and applications, Prog. Polym. Sci. 39 (2014) 683–706, https://doi.org/10.1016/j.progpolymsci.2013.07.006.

[20] S. Brunauer, P.H. Emmett, E. Teller, Adsorption of gases in Multimolecular Layers, J. Am. Chem. Soc. 60 (2) (1938) 309–319, https://doi.org/10.1021/ja01269a023.

[21] D.H. Everett and J.C. Powl. Adsorption in slit-like and cylindrical micropores in the henry's law region. A model for the microporosity of carbons. J. Chem. Soc., Faraday Trans. 1. 72 (1976), 619–636. Doi: 10.1039/F19762000619.

[22] B. Singh Tomar, A. Shahin, M.S. Tirumkudulu, Cracking in drying films of polymer solutions, Soft Matter 16 (2020) 3476–3484, https://doi.org/10.1039/C9SM02294E.

[23] S. Paramee, R. Guo, A.S. Bhalla, H. Manuspiya, A comparison of shear-mixing and solvent-induced on phase behavior, thermal and dielectric properties of PVDF-HFP/MOF composites, J. Appl. Polym. Sci. 139 (2022) e52741.

[24] D. Cheng, L. Zhao, N. Li, S.J.D. Smith, D. Wu, J. Zhang, D. Ng, C. Wu, M. R. Martinez, M.P. Batten, Z. Xie, Aluminium fumarate MOF/PVDF hollow fiber membrane for enhancement of water flux and thermal efficiency in direct contact membrane distillation, J. Memb. Sci. 588 (2019) 117204, https://doi.org/10.1016/j.memsci.2019.117204.

[25] L.R. Redfern, O.K. Farha, Mechanical properties of metal–organic framework, Chem. Sci. 10 (2019) 10666–10679, https://doi.org/10.1039/c9sc04249k.

[26] I. Tournis, D. Tsiourvas, Z. Sideratou, L.G. Boutsika, A. Papavasiliou, N.K. Boukos, A.A. Sapalidis, Superhydrophobic nanoparticle-coated PVDF-HFP membranes with enhanced flux, anti-fouling and anti-wetting performance for direct contact membrane distillation-based desalination, Environ. Sci. Water Res. Technol. 8 (2022) 2373–2380, https://doi.org/10.1039/D2EW00407K.

Glossary

MOF: Metal Organic Framework
Al-fum: Aluminium fumarate
PVDF-HFP: poly(vinylidene fluoride-co-hexafluoropropene)
MMM: Mixed Matrix Membranes
MW: Molecular Weight
d: density
DMF: Dimethylformamide
SSA: Specific Surface Area
BET: Brunauer, Emmett and Teller
HK: Horvath-Kawazoe
SEM: Scanning Electron Microscopy
ASTM: American Society for Testing Materials
TS: Tensile Strength
SCA: Static Contact Angle
IUPAC: International Union of Pure and Applied Chemistry
STP: Standard Temperature and Pressure
DSC: Differential Scanning Calorimetry
XRD: X-Ray Diffraction